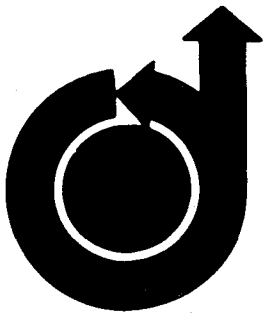

AIAA Paper
No. 73-1300

SOME EXPERIMENTS RELATED TO L-STAR INSTABILITY IN ROCKET MOTORS

by
R. N. KUMAR and R. P. McNAMARA
Guggenheim Jet Propulsion Center
Pasadena, California

AIAA/SAE 9th
Propulsion Conference
LAS VEGAS, NEVADA / NOVEMBER 5-7, 1973

First publication rights reserved by American Institute of Aeronautics and Astronautics. 1290 Avenue of the Americas, New York, N. Y. 10019. Abstracts may be published without permission if credit is given to author and to AIAA. (Price: AIAA Member $1.50. Nonmember $2.00).

Note: This paper available at AIAA New York office for six months; thereafter, photoprint copies are available at photocopy prices from AIAA Library, 750 3rd Avenue, New York, New York 10017

-- NOTES --

SOME EXPERIMENTS RELATED TO L-STAR INSTABILITY IN ROCKET MOTORS*

R. N. Kumar** and R. P. McNamara†
Daniel and Florence Guggenheim Jet Propulsion Center
California Institute of Technology, Pasadena, California

Abstract

The influence of condensed phase heterogeneity on the L^* instability of nonmetallized AP/PBAN propellants is explored using four propellants (with monomodal AP particle distributions having 50 per cent weight average points at 11, 39.5, 175, and 350 microns). An economical firing program is used. One-dimensional nature of the Helmholtz mode and the complex nature of the chuff mode are revealed through color movies. The stability boundary on the L^*-pressure plot is found to be parabolic. Frequency correlations and many other features reveal the important role of condensed phase details in propellant combustion.

I. Introduction

The extreme simplicity of the solid propellant rocket motor is counterweighed by the instability problem when practical applications are considered. To a large extent, the difficulty with the instability problem is no doubt associated with a lack of knowledge regarding the fundamental combustion processes. The situation should improve with more research effort. However, another factor of great relevance is the lack of good experimental data covering the unstable operation of full-scale rockets. Data on actual rocket instability, even if made available, would be difficult to process because of the complex combinations of the parameters involved. Thus, experiments are to be conducted where the parameters are isolated and their variations are controlled.

Quite often, an experimental work planned to yield meaningful scientific information appears to be rather isolated from contemporary rocket technology. Research on the oxidizer and the fuel separately, nonmetallized propellants, unimodal oxidizer distributions are typical examples. However, the benefits from such fundamental work, planned to lead into the close neighborhood of actual rockets, are to be appreciated. Frequently, the results from even the initial stages of such a long range program are directly applicable to actual rocket propellants, thereby enhancing the value of such research.

The present work was undertaken to obtain data from tests, where the influence of the compositional variables (in propellant formulation) on instability behavior are explored. The compositions of the state-of-the-art solid propellants are extremely varied. In order to understand, in a non-empirical manner, the effects of compositional variations, the simplest of experiments was designed. Only a single compositional parameter was varied, and the propellants were fired under very similar motor conditions.

The two primary aspects of the present research effort, namely the propellants and the instability mode, are briefly discussed below. The propellant chosen must be readily unstable and must possess a simple composition. Previous experience at JPL had indicated that the NWC A-13 propellant is one that exhibits oscillatory combustion readily. The composition of the A-13 is 76% AP 24% PBAN. Among the various parameters that characterize propellant formulation, a single parameter was chosen to be varied over a significant range. Oxidizer particle size was chosen as having significant influence over the ballistic properties, besides being a simple parameter. Assuming complete combustion, the far-downstream quantities (flame temperature, species fractions, etc.) are not affected by oxidizer particle size. Steady-state linear regression rates of many propellants have been known to be significantly affected by the AP particle size. Oscillatory combustion characteristics are also known[1,2] to be affected, although a systematic study of the influences of this single parameter is not readily available.

Ideally, one would like to have a truly unimodal distribution of spherical particles of AP. In practice, easy availability dictated the choice. The distributions used in the present study are shown in Fig. 1, where the propellants (and the names of the propellants) are also seen. The $\tilde{A}$-13 propellant used here was cast at JPL, as contrasted with the standard A-13 of NWC. In order to maintain a consistent nomenclature, the 50 per cent weight point has been used to identify a distribution. Thus, 11μ, 39.5μ, 175μ, and 350μ are the oxidizer particle sizes associated with the propellants CIT-2, $\tilde{A}$-13, CIT-3, and CIT-4, respectively.

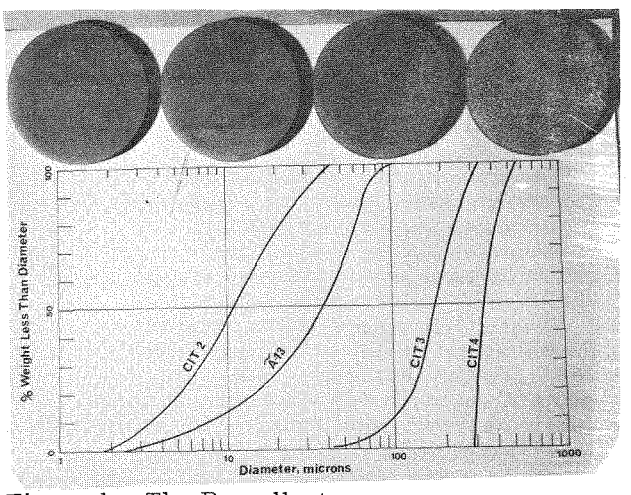

Figure 1. The Propellants.

Since the basic aim was to understand the manner in which the instability behavior of solid propellants would be affected by variations in propellant formulation, the simplest instability mode

*This work was supported by NASA under the Jet Propulsion Laboratory contract NAS 7-100.

**Research Fellow in Jet Propulsion.

†Undergraduate student, Applied Physics.

for examination was chosen as the familiar L-star mode, where the oscillations occur simultaneously in the bulk of the chamber leading to the earlier nomenclature "bulk mode instability" or "Non-Acoustic Instability" -- NAI. (It has since been theoretically clarified[3, 4], however, that the oscillations are the zeroth mode in a standard sequence of acoustic modes.) The L^* oscillations have been observed at relatively low pressures (a few atmospheres). Low pressures simplify the experimental set up.

Of the two principal modes of unstable combustion (namely, chuff and Helmholtz), the Helmholtz mode is found to be ordered, and hence maximum attention is given to its understanding.

Motion pictures through a transparent motor show the one-dimensional nature of combustion during the Helmholtz mode. The frequency of these oscillations is found to bear a much stronger relation to the characteristic residence time ($a/\bar{r}$) in the condensed phase than to the characteristic heat transfer time ($\varkappa/\bar{r}^2$). Also, simple correlations of the frequency with the chamber characteristic length (L^*) are found to be of limited validity only.

The stability boundary, on the L^*-$\bar{P}$ plot, is found to be parabolic in shape, although experimental difficulties prevented the obtaining of the full locus for all four of the propellants. The high pressure limit for unconditional stability is predicted based on the postulated importance of the role of the condensed phase as a heat reservoir. The agreement is found to be excellent for the CIT-2 (11μ) propellant, but less convincing for the other three.

The amplitudes of the pressure oscillations are found not to correlate satisfactorily with any of the chamber or propellant variables. The closest correlation is with a parameter based on the concept of volumetric energy release rate in the chamber.

Many features of the finest oxidizer particle propellant (CIT-2) are found to be significantly different from those of the other three even on a qualitative basis. Also, many of the variations in the dynamic characteristics (normalized frequency, for example) are not monotonic with the oxidizer particle size variations.

The chuff mode combustion is revealed, by color movies taken through a transparent chamber, to be far from one-dimensional or steady. The events behind a chuff (a pressure spike) are found to be random and statistical in nature.

Finally, the role of the condensed phase details in unstable combustion is repeatedly emphasized in the present work, both during the testing phase and during the data processing phase. The extensive experimental data now invite theoretical research efforts.

II. TEST FACILITY AND INSTRUMENTATION

The test facility consists of the L-star burner, control and data acquisition instruments. The burner (Fig. 3) is a $2\frac{1}{2}$" (inside diameter), 5" long cylindrical chamber (C) with a nozzle end plate (N) and a piston end plate (E). The propellant

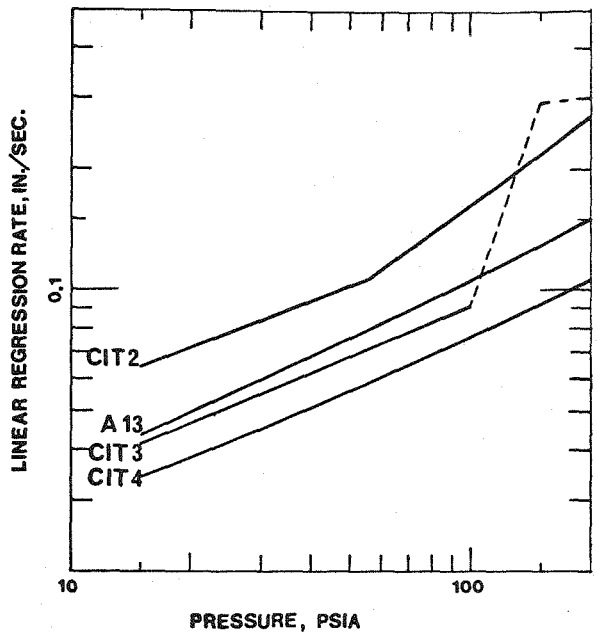

Figure 2. Crawford Bomb Data on the Propellants.

disc is bonded to the piston (P) which is mounted at the end of a centrally-located screwed rod, the axial position of which enables the selection of different chamber volumes. The assembled view is shown in Fig. 4, where the propellant surface coated with the ignitor paste is seen through the transparent nozzle end plate. The transparent end plate was used only in a few of the runs, when flow visualization inside the chamber was desired. All other tests used the stainless steel nozzle end plate.

The data acquisition instrumentation consisted of a pressure transducer (Taber gauge; Teledyne models 217-SA, 0-100 and 176-SA, 0-300 psi) that communicates with the chamber through a short length (approximately 3") of 1/4" stainless steel tubing. Distortion of the pressure signal through the tubing should be negligible considering that only bulk-mode oscillations are encountered. The electrical output from the Taber gauge was passed through an amplifier (General Dynamics, D. C. - 10 Hz, flat) and recorded on a CEC 5-124 oscillograph. A Tektronix storage oscilloscope was connected in parallel with the oscillograph to obtain a time-compressed display of the pressure history.

Early in the program, the need was recognized for visually observing the motor during a firing. Visual observation of the exhaust provides the least misleading indication of the termination of a run. Such information is necessary for stopping the recording instruments. A closed-circuit TV was used for this purpose.

III. TEST PROCEDURE

In this section the details of mounting the propellant, selection of the operating conditions and ignition are described. Some of these details have a profound influence on the data obtained and also on the interpretation of data.

3.1 Propellant Mounting

The propellant discs were invariably bonded

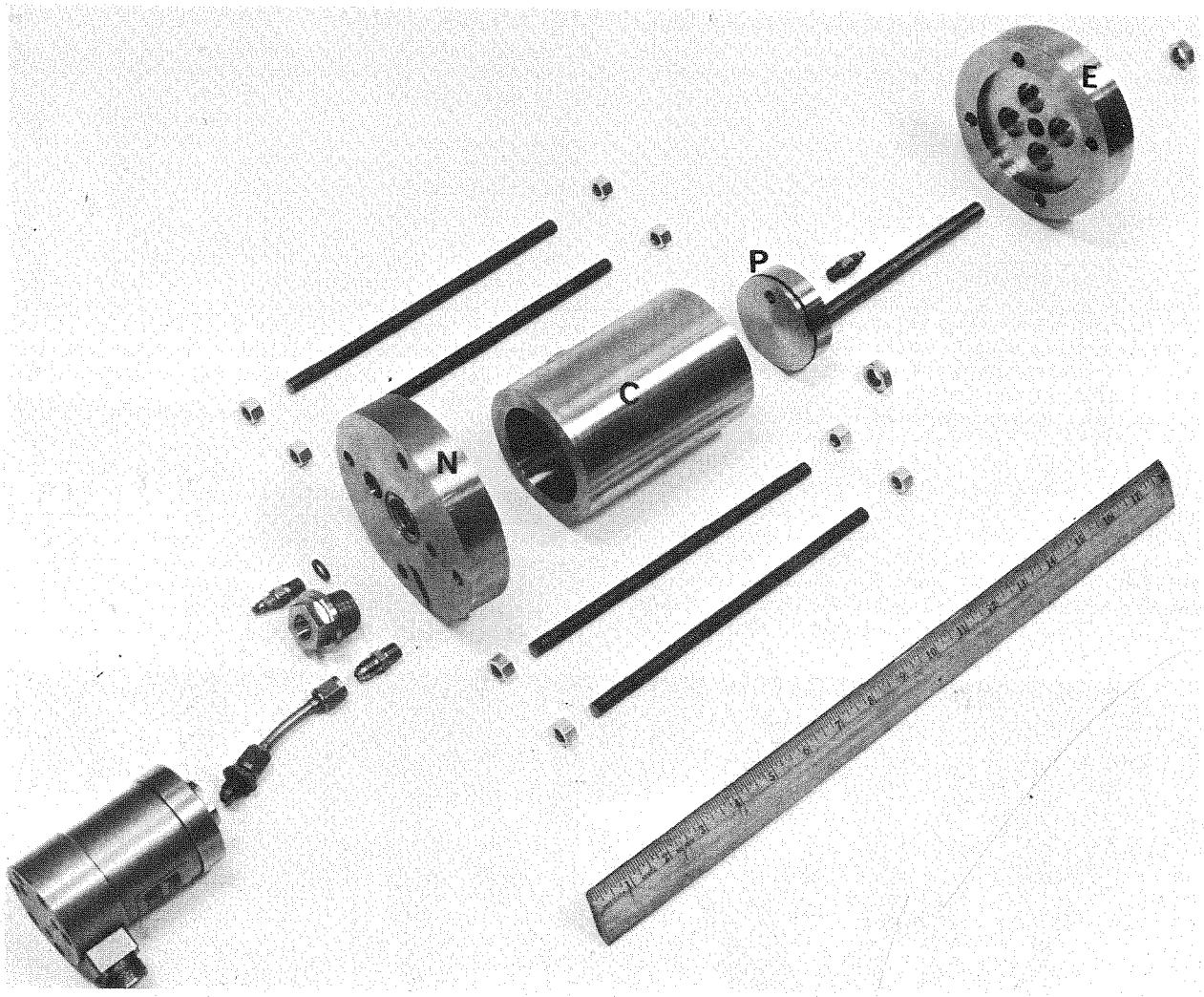

Figure 3. The L* Motor Disassembled.

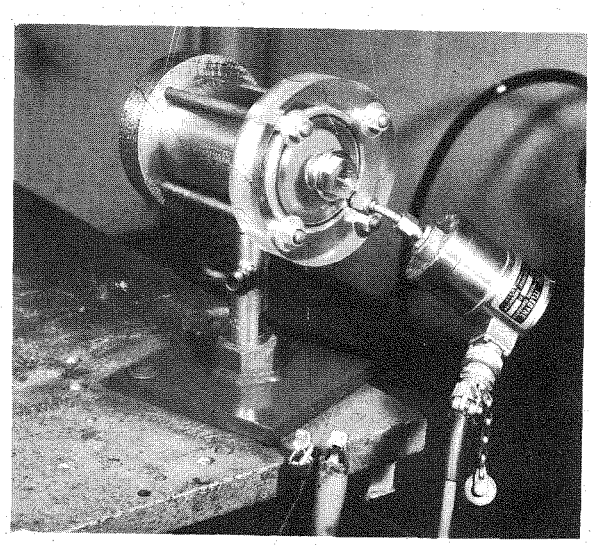

Figure 4. The L* Motor Assembled.

to the stainless-steel piston (P, Fig. 3) with the EPON resin (5 parts of Shell 828 resin with 1 part of curing agent D). The bond received cure for $2\frac{1}{2}$ hours in an oven maintained around 140°F. Thus, the propellants received a cure of $2\frac{1}{2}$ hours in excess of their 160-hour cure following casting. A few of the runs during the early part of this program had the propellant edges inhibited with the same EPON resin. The procedure proved to be both unsatisfactory and unnecessary. The tolerances in the machining of the combustion chamber C (Fig. 3) are such that even the thin (≈0.01") layer of hard resin on the edge of the propellant prevented the easy assembling of the motor. Secondly, the edge of the propellant is so close to the cold wall of the chamber that no combustion over the edge seems plausible. Lastly, no experimental evidence indicated that edge burning (i.e., radial regression of the propellant) was significant even when the edge was not inhibited. Several of the tests got terminated before the propellant was fully consumed during a firing, and a scrutiny of the semi-consumed propellant gave no visible evidence of radial regression.

3.2 Experimental Variables

The two primary variables are the nozzle

throat diameter (D^*) and the chamber free volume (V_c). The D^* sets the chamber pressure during time-independent burning of any given propellant for a specific burning area. The chamber free volume, for a given D^*, sets the motor characteristic length (L^*) by the very definition

$$L^* = \frac{\text{Chamber Free Volume } (V_c)}{\text{Nozzle Throat Area } (\pi D^{*2}/4)} .$$

The pressure-time history of a run is strongly influenced by these two variables D^* and L^*. For convenience, we use the variable P_c (mean chamber pressure) to signify variations in inverse D^*, being fully aware that such a usage is strictly justified only during steady burning of the propellant. In order to have a clear feel for the overall behavior, Fig. 5 has been composed from actual test records obtained on the storage oscilloscope. At low values of L^* and P_c, pressure spikes are seen (Fig. 5a). The motor is said to be chuffing. At high values of L^* and P_c, time-independent burning is observed (Fig. 5c). This mode is characterized by an almost constant mean value of the chamber pressure that varies only randomly at the intrinsic "noise level" characteristic of the propellant.

At intermediate values of L^* and P_c, regular pressure oscillations are observed around a mean value (Fig. 5b). These are the bulk-mode or Helmholtz oscillations in the chamber. If we expand the pressure record in time, almost sinusoidal oscillations are revealed. (In the literature the term "L^* instability" is frequently reserved exclusively for these Helmholtz oscillations.) These are the three fundamentally different pressure signatures obtained in an L^*-burner. As a slight variation, we often see the "pressure burst" phenomenon, where the rapidly-growing Helmholtz oscillations are abruptly terminated on reaching a sufficiently high amplitude, resulting in a depressurization extinguishment, following which the chamber pressure falls to zero. Representative run records of this phenomenon are shown in Fig. 6.

In order to understand the L^* instability behavior as fully as possible, it was desired to vary the two primary variables (L^* and P_c) over as wide a range as feasible. Presumably, at any value of P_c, the L^* value would be varied over the range that takes the motor from chuff mode (low L^*) through Helmholtz mode (medium L^*) to steady mode (high L^*). In order to do this, the chamber free volume has to be varied from a low value to a

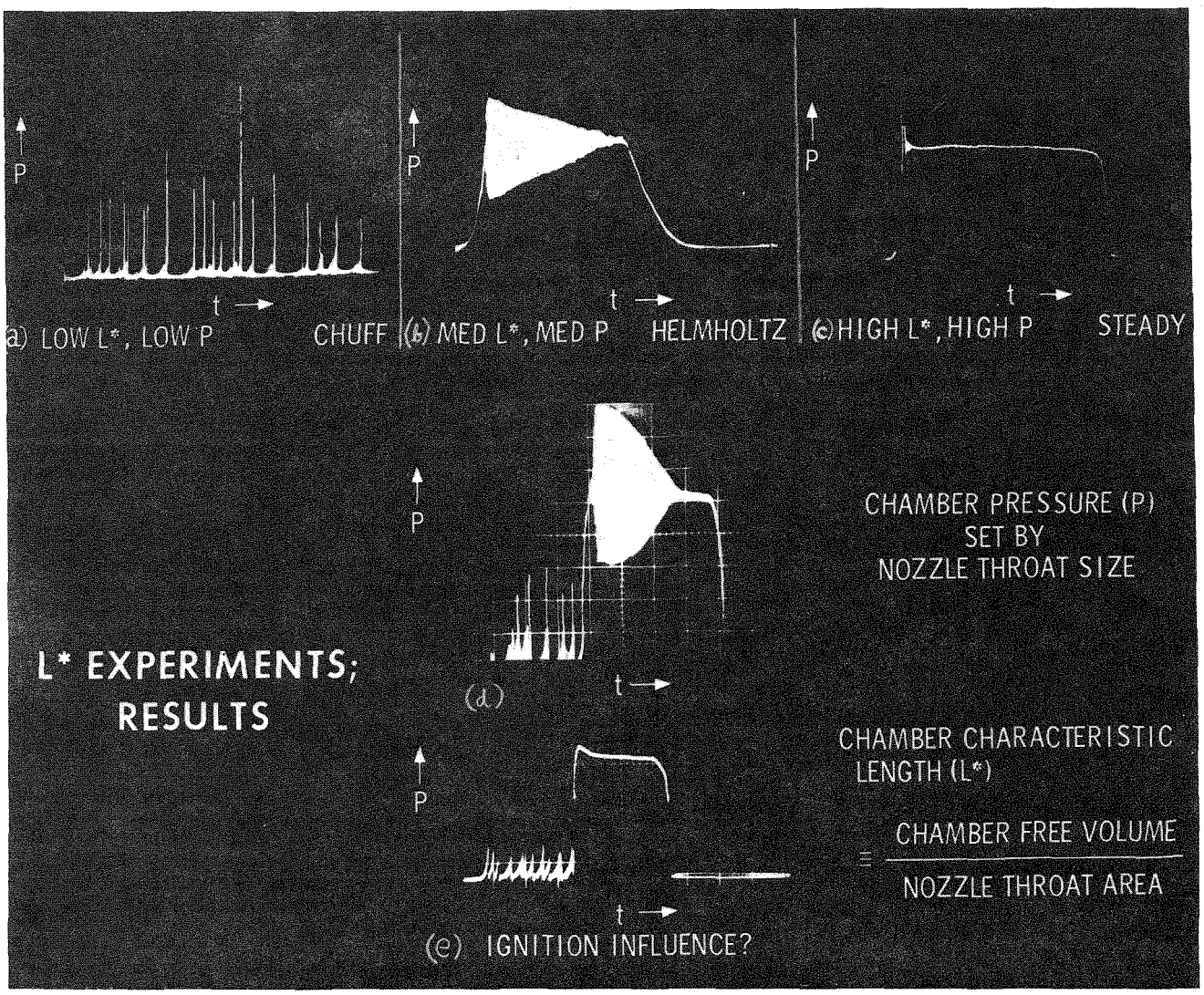

Figure 5. Results of L^* Experiments.

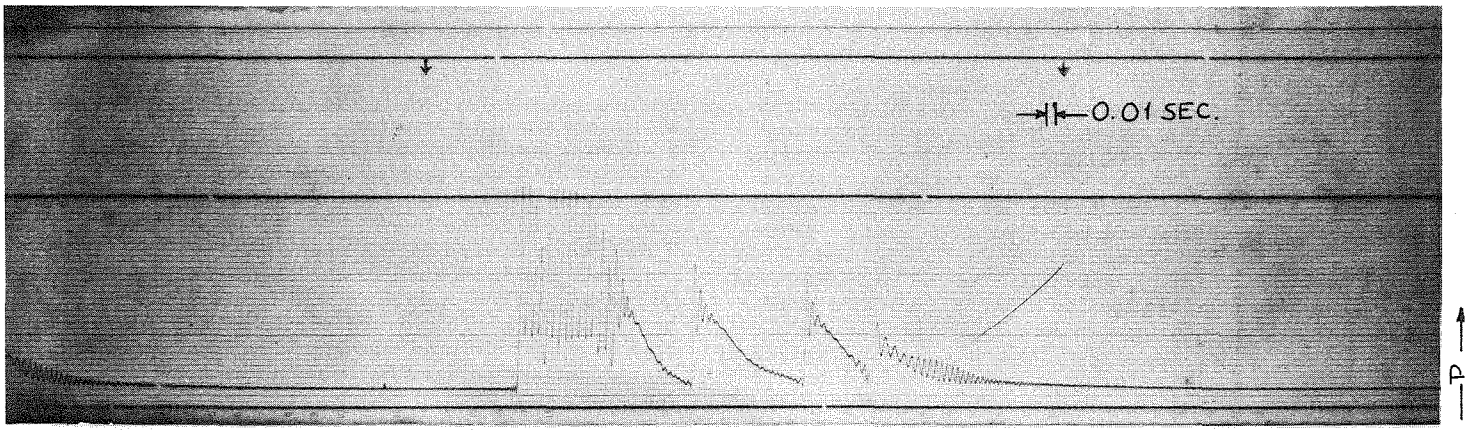

(a) CIT-2 Propellant Run No. 34

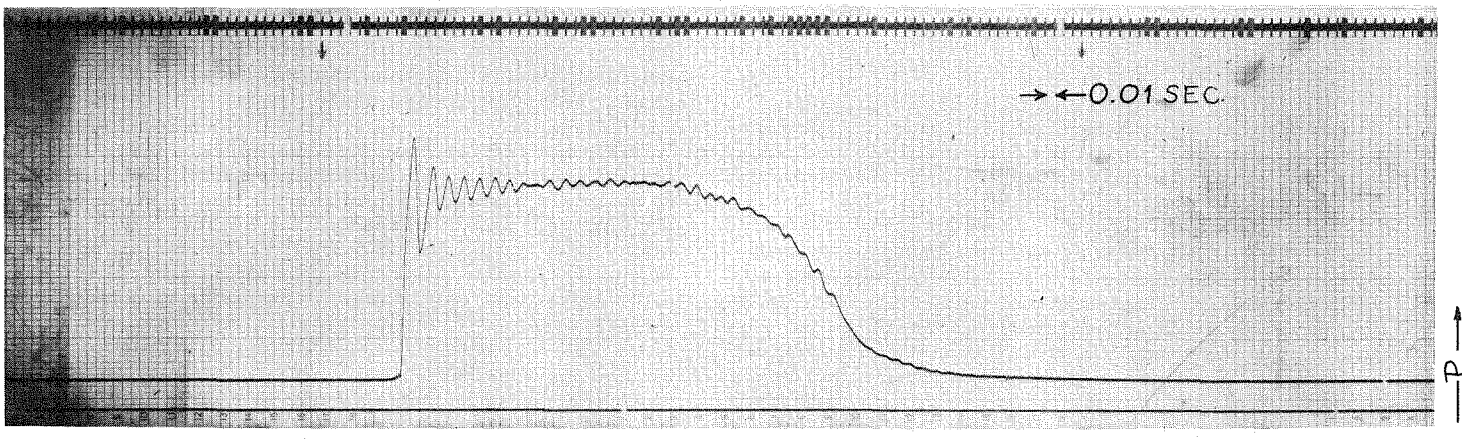

(b) $\widetilde{A}$-13 Propellant Run No. 155 ←Time (t)—

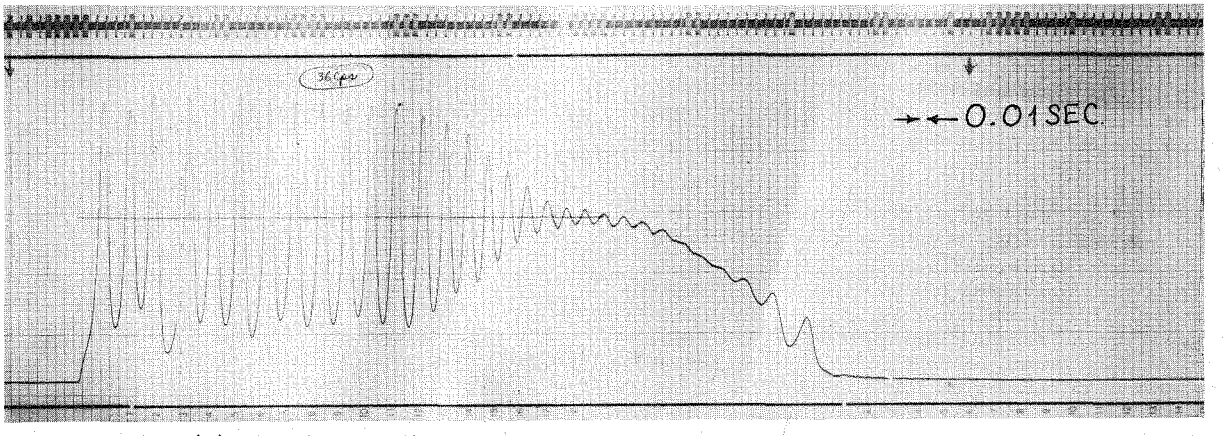

(c) CIT-3 Propellant Run No. 71 ←Time (t)—

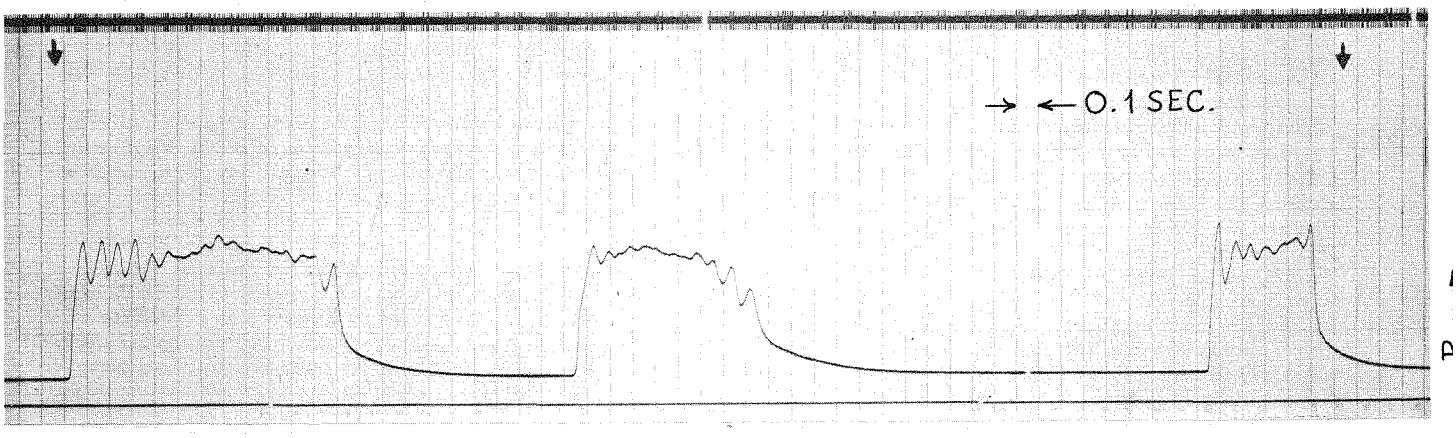

(d) CIT-4 Propellant Run No. 173 ←Time (t)—

Fig. 6 Typical Signatures of the Four Propellants in the Depressurization Rate ($\frac{dP}{dt}$) Extinguishment Mode

high value for any given P_c. Such a variation is possible during a single firing, when one recognizes that the chamber free volume is increasing during a run because of the depleting propellant volume. The initial propellant volume and chamber free volume are adjusted such that the three fundamentally different modes of motor operation are encountered in a single firing. The actual values to be used in testing a propellant have to be arrived at after one or two exploratory runs. However, an actual test lasts a maximum period of 30 seconds (a majority of them between 5 and 10 seconds), while the preparation for a test lasts approximately 30 minutes in addition to the $2\frac{1}{2}$ hours cure time for the bond. Thus, great economy in testing can be achieved by covering the full range of L^*'s of interest in a single firing.

3.3 Ignition

During the course of these investigations, some interesting details of propellant ignition were revealed. Also, the widely recognized importance of ignition to rocket motor operation was confirmed.

The objective of ignition is to start the combustion of the propellant in a uniform manner all over the propellant surface simultaneously. In the selection of the actual ignition procedure, an earlier work[5] at JPL provided valuable guidance. Different methods of propellant ignition had been compared in T-burner firings, and a method that proved to yield consistently good results used a centrally - located ignitor pellet over the propellant surface coated with a layer of the ignitor paste. The central pellet, upon ignition (through electrical heating of a nichrome wire located at the core of the pellet), sprays hot particles symmetrically over the layer of ignitor paste on the surface of the propellant, and ignition is initiated, fairly symmetrically, at several different spots. This results in a rapid and uniform ignition of the propellant.

Two different ignitor pastes were used in the present experiments. One of them, generously supplied by the Naval Weapons Center, goes by the name of X-225 and has the following composition: polyisobutylene, 6.0 wt. percent; boron powder, 6.9 wt. percent; titanium powder, 14.8 wt. percent; potassium perchlorate, 72.3 wt. percent. The other ignitor paste, formulated at JPL, is named CIT IP 1 and has the following composition: polyisobutylene, 7.0 wt. percent; boron powder, 6.0 wt. percent; aluminum powder, 14.0 wt. percent; ammonium perchlorate 73.0 wt. percent. CIT IP 1 was originally intended as a substitute for the NWC X-225, but revealed such poor mechanical and handling characteristics compared to X-225 that it was discarded in favor of the latter. However, as the experiments progressed, CIT IP1 proved invaluable for the ignition of the propellants with coarser oxidizer particles. It must be recalled that the burning rates of the propellants decrease in the order of increasing coarseness of oxidizer particles (Fig. 2). The X-225 ignitor paste, while very successful in the ignition of CIT-2 propellant (11μ AP particles) and also successful in the ignition of the A-13 propellant (39.5μ AP particles), burned too fast for the CIT-3 (175μ AP particles) and CIT-4 (350μ AP particles) propellants. That is, upon ignition of the central pellet, the layer of X-225 on the surface of the propellant burned out quickly, while the propellant never had sufficient time for ignition. The need was felt for a slower-burning ignitor paste. The readily available CIT IP 1 was employed for coating the propellant surface after recognizing that aluminum is slow burning at the low pressures encountered. This choice proved highly successful and, in fact, made all the difference in our ability to get the CIT-3 and CIT-4 propellants to ignite at low chamber pressures. (Exposure of fresh oxidizer particles in the propellant, through a mild abrasion of the propellant surface before applying the coat of ignitor paste, proved helpful at times.)

Thus, the thought emerged that for satisfactory ignition of propellants, we need an ignitor paste, the characteristic combustion time of which is not too different from the characteristic combustion time of the propellant itself. This empirical information, obtained during the present program, has proved very useful so far.

Except for the choice of the surface layer of ignitor paste as noted above, an attempt was made to maintain a standard ignition technique in all of the firings. The thickness of the surface layer could have varied (around 0.01") from run to run, but not by much. Also, the size of the central ignitor pellet was varied a little in order to obtain satisfactory performance as dictated by experience. As a general rule, smaller pellets were needed for smaller volumes of the combustion chamber. This is probably due to a depressurization rate effect. The gas produced upon ignition of the ignitor paste has to vent through the nozzle. The venting process produces a (dp/dt) transient in the combustion chamber that could become severe enough to extinguish the propellant (if it is already lit). A smaller pellet, producing less gas, results in a smaller (dp/dt) transient for a given chamber condition, and the propellant could remain lighted during such a transient.

The most interesting result of the variation in pellet size was the complete suppression of the Helmholtz mode oscillations on occasions. The motor went from the chuff mode at low L^* values into the steady mode at high L^* values through the steady mode at intermediate L^* values, instead of through the Helmholtz mode. This different is strikingly displayed in Figs. 5d and 5e. It would appear that even when the conditions in the motor are suitable for Helmholtz oscillations, a large amplitude disturbance (such as available during the final stages of a violent chuff mode) may be necessary for exciting the Helmholtz mode oscillations. The implications of such a nonlinear behavior are not clearly understood. As a matter of fact, the very phenomenon was found not to be readily reproducible. It presumably depends on small, as yet obscure, details of chamber conditions. More research is needed to shed light on the situation. The importance of such research is readily appreciated when one recognizes the possibility of totally suppressing chamber pressure oscillations.

It is noted in passing that a careful record has been maintained of the precise details of the ignition technique used in every one of the firings, so that any future study pertaining to correlations of test results with the ignition technique has available the data to work from.

3.4 Volume Measurement

After a test was over (even if the propellant was not fully consumed during the run), the chamber volume was measured by filling the chamber with water from a graduated jar. Throughout the present report, the combustion chamber volume (V_c) is implied to signify the free volume of the chamber up to the throat of the nozzle. The error in the volume measurement is estimated to be within ± 0.5 cc. The measured volumes ranged from 20 cc. to 200 cc.

IV. STUDIES IN A TRANSPARENT MOTOR

In this section, some visual observations in the L^* motor are described. The observations helped to clarify certain features of L^* instability. The observations clearly showed the ignition sequence, luminosity variations during Helmholtz instability, and the complicated nature of the chuff-mode combustion.

4.1 The Experimental Setup

A transparent nozzle end plate was machined from a 1" thick block of plexiglas. The very low cost of the material, together with easy machineability, led to the choice of plexiglas. It was recognized that the poor heat resistance characteristics of the material may obscure details inside the chamber during visual observations. However, cost considerations ruled out the possibility of quartz windows and inert gas purge over the wall. Besides, the deterioration in the transparency of the plexiglas end plate was not expected to commence until after the heavy flow of combustion gases over it. Thus, the details, at least during ignition and the initial stages of a chuff, were anticipated to be seen clearly. Later observations revealed not only the limited details anticipated but extensive details of the chuff mode as well, for reasons that should be obvious shortly.

The assembled L-star burner with the plexiglas end plate was shown in Fig. 4. A Hycam Model 400 motion picture camera was stationed with its lens approximately three feet away from the nozzle end plate. Motion pictures were taken on Kodak Ektachrome film of two separate firings. The first (run no. 32) exhibited strong Helmholtz oscillations but no chuffing; the pictures were taken at 4000 frames per second. The second firing (run no. 33) exhibited several chuffs before entering the time-independent combustion mode. No Helmholtz oscillations were observed; the motion pictures were taken at 3000 frames per second. The originals of the processed films are with Section 381 at the Jet Propulsion Laboratory. Several prints taken from the movie frames, and presented in this report, are described below.

4.2 The Helmholtz Mode

The Helmholtz oscillations were revealed as cyclic luminosity variations in the movie. One complete cycle is presented in Fig. 7. To orient the reader with respect to the camera, it is observed that the movies are taken from exactly the same relative position from which Fig. 4 was taken.

The ignitor leads (31 gage copper wires) are seen on the left of the nozzle in all of the frames.

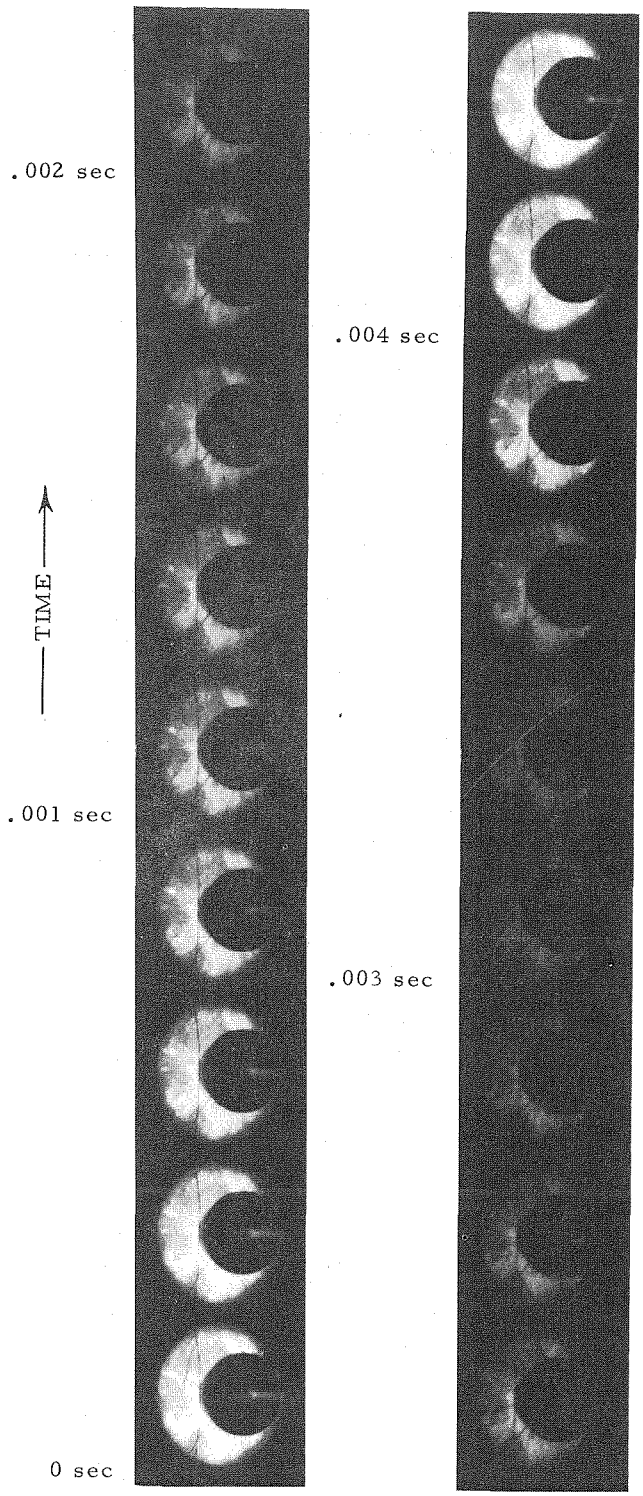

Figure 7. The Helmholtz Mode (run no.32, Propellant CIT-2).

Another feature common to all of the frames in Fig. 7 is the inhomogeneous appearance of luminosity. The origin of this "patchy" appearance is the non-uniform erosion of the plexiglas on the inside surface. The invariable spatial variations during ignition (when the hot particles emanate from the central pellet) are believed to be among the prime causes of the asymmetric erosion pattern of the plexiglas. (Minor variations in the thickness of the silicone grease on the inside sur-

face could be another factor.) The point of these observations is that the inhomogeneous luminosity pattern seen in the frames is due to the plexiglas erosion pattern and not due to inhomogeneous luminosity inside the chamber. This fact can be appreciated by following the entire sequence of events (beginning with ignition) in the movie. In Fig. 7 it is suggested that some specific spot (spatial location) be followed from frame to frame. It is seen that only the light intensity varies and not the general pattern around such a spot. The lack of spatial variations inside the chamber is taken to signify the one-dimensional nature of combustion during the Helmholtz oscillations.

An interesting feature seen both in the movie and in Fig. 7 is that the luminosity variations do not possess symmetrical growth and decay patterns. While the growth needs approximately one millisecond (4 frames), the decay is spread over approximately three milliseconds (12 frames). The pressure oscillations recorded on the oscillograph at a paper speed of 16" per second indicate that the waveform is apparently symmetrical. However, one of the tests (run no. 39) on the CIT-2 propellant had its data recorded at 64" per second, which reveals the actual waveform with much greater clarity. As seen in Fig. 8, the pressure oscillations are indeed asymmetrical and conform rather closely to the luminosity oscillations. The asymmetrical oscillations are among the several exclusive features observed with the CIT-2 propellant, as discussed later. The other three propellants reveal nearly symmetrical oscillations as may be seen in Figs. 6 b, c, d and Figs. 11 a, b.

4.3 The Chuff Mode

The chuff mode was revealed as high-activity periods, isolated in time, superposed on a general background of very low activity in the chamber. Such a picture was fairly evident from the earlier pressure traces; but what was not evident from the pressure traces was the nature of the low-activity background in the chamber, which was clarified by the movie photographs.

During most of the ignition sequence, very little difference was found between this run (no. 33) and the one that exhibited Helmholtz instability (no. 32). However, towards the end of the ignition sequence, it was observed in the motion pictures that no luminous area (the "flame") covered the surface of the propellant, in contrast with the earlier run. Isolated bright spots were seen, and these were identified as the hot metal particles from the ignitor paste. (It is to be remembered that the propellant itself is non-metallized.) Following the actual sequence of events, surface distortions of the propellant became perceptible. Isolated regions of subdued brightness (nowhere near the brightness of a full flame over the surface) were seen. The bright metal particles were seen to circulate slowly around the circumference of the chamber, possibly signifying the existence of mild eddying motion of vapors inside the chamber.

If relative motion occurred between the hot metal particles and the surrounding vapors, it must have been in the Stokes/Oseen regime. Occasionally the isolated regions of subdued brightness gave rise to a brighter gas evolution that discharged through the nozzle in a "puff," presumably corresponding to a chuff in the pressure-time trace shortly before the discharge.

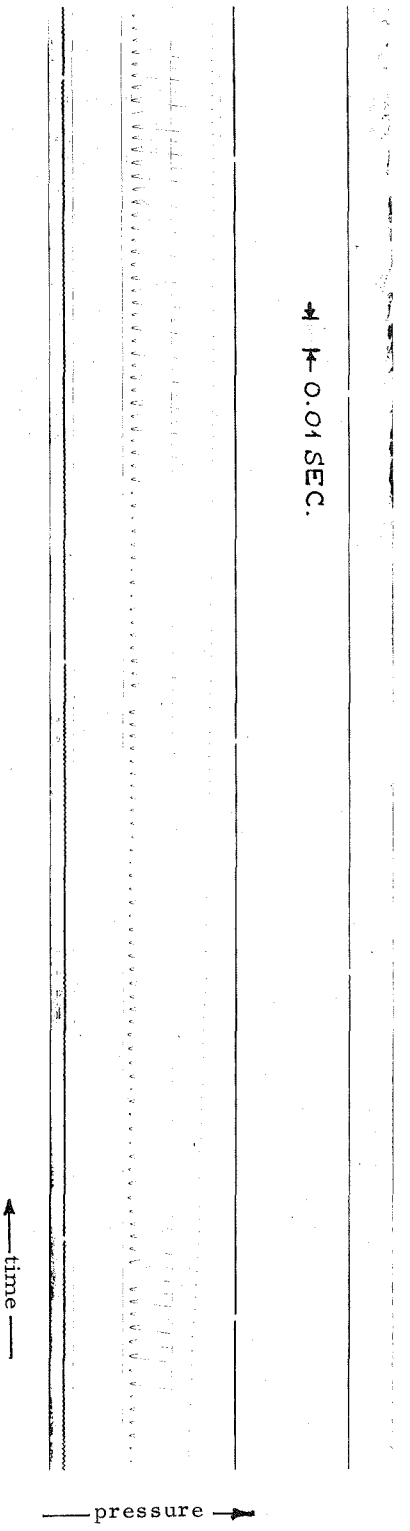

Figure 8. Extended-time Pressure History of the CIT-2 Propellant. Asymmetric Waveform Is Evident. Run No. 39.

All these activities took place in the chamber, with the general background being fairly dark. At no time during the entire sequence of these events was there a heavy evolution of combustion gases

uniformly from the propellant surface. The lack of erosive flow of hot gases over the plexiglas nozzle end plate kept the plate fairly transparent all through these events and afforded a visibility that was better than expected.

Even when the propellant was not burning in the normal manner, evolution of vapors from the propellant surface was evident in isolated areas. This mass loss, even in the absence of steady burning, can introduce large discrepancies between the regression rate calculated on the basis of total chuff duration and propellant thickness variation, and the regression rate measured in a bomb. The increasing chamber volume (due to the depletion of the propellant volume), and hence the increasing L-star, finally placed the propellant in the steady-burning mode, after which event Fig. 9a was obtained. This photograph is to be compared with those obtained during the Helmholtz mode in the previous run (Fig. 7). The point is to note the general uniformity in luminosity inside the chamber, although the view is a little obscured due to plexiglas erosion (already discussed).

Figure 9a. Time-independent combustion. Uniform glow. Choked nozzle.

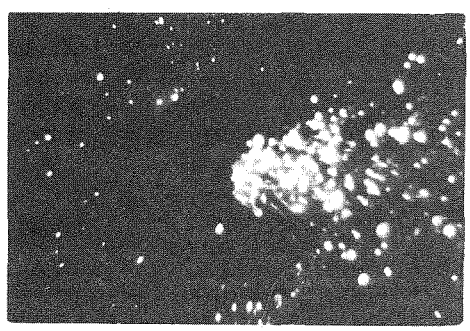

Figure 9b. Early stages of ignition. Spray of hot metal particles from the ignitor paste.

Figure 9c.

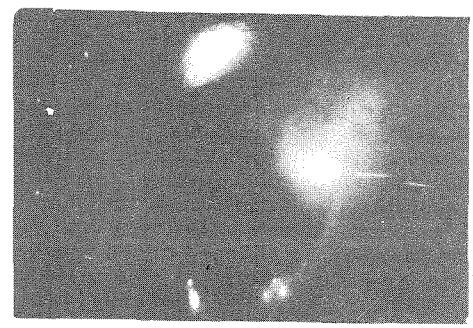

Figure 9d.

Figure 9e.

Figure 9. Details of a Run with Chuff-Mode (Run No. 33; 3000 frames per second).

During the initial stages of ignition, Fig. 9b was obtained. As well as can be judged, the bright metal particles are seen with as much clarity inside the chamber as outside the chamber, indicating that the plexiglas platehas not yet suffered erosion. Figures 9c, d, and e were obtained during various stages of the chuff mode operation. It is readily appreciated that there does not exist a uniform combustion zone over the propellant surface. The isolated regions of activity are also seen. These frames were specially chosen to reveal the "puff" of hot gases leaving the nozzle. This is to be compared with the supersonic exhaust (which results in a visible shock after nozzle exit) during normal combustion in Fig. 9a. In comparison with the prints in Fig. 9, we note that the details of surface distortion are far more clear in the original movie. Nevertheless, the prints should indicate the general features described earlier.

Based on these observations, an overall description of the chuff-mode operation is attempted as follows. For some poorly understood reason, the $L^* - D^*$ combination places the propellant in a regime where non-uniform combustion over the surface is possible. The local heating of the propellant causes both severe mechanical distortions and evolution of vapors locally. If these vapors happen to have available an ignition source, such as a hot metal particle from the ignitor paste, local combustion of this mass of vapors gives a momentary surge of pressure in the chamber. A rapid depressurization follows the exhaust of this mass of burned gas. The observation that the combustion of this mass of gas does not initiate the familiar "flame" uniformly over the propellant surface until after the L^* has increased to a sufficiently large value needs further study.

One fact that emerges unmistakably from these studies is that combustion near the propellant surface during the chuff-mode operation is far from being one-dimensional or steady. Any realistic analysis of the chuff mode will have to incorporate these essential features. Another aspect is the possible contamination of the chamber gases with ambient air due to the very low flow rate of propellant vapors (burned or unburned) through the nozzle from the chamber. This feature is obviously absent during choked flow observed when the propellant is burning normally.

Two tests on the propellant CIT-2 conducted under practically identical conditions of L^* and D^* need special mention. In run no. 37, a very thin layer of ignitor paste was applied over the propellant surface and a small ignitor pellet was employed. The ignition variables were chosen so as to create as small a pressure disturbance as possible and were naturally conducive to poor ignition of the propellant surface. From the foregoing description of the chuff-mode operation, we might expect that the poor ignition would result in chuffs, if the $L^* - D^*$ combination permits them. In the oscilloscope trace obtained during the run (Fig. 10a), chuffs are visible as anticipated, and also no Helmholtz mode is evident.

Run no. 38 employed a thick layer of ignitor paste over the propellant surface and also a very large ignitor pellet. The ignition variables here were chosen so as to give as uniform an ignition as possible, and were naturally conducive to the occurrence of large pressure disturbances in the chamber. As seen in the oscilloscope trace presented in Fig. 10b, the chuff mode was totally eliminated, but the Helmholtz mode got initiated.

While these observations support both the postulated influence of ignition on the chuff mode and the nonlinear nature of the Helmholtz mode, quantitative correlations are very difficult. Quantitative correlations form the basis of a theory, and also enable us to usefully employ these observations in an actual rocket motor, at least in an empirical manner.

V. EXPERIMENTAL DATA AND INTERPRETATION

The interpretation of pressure traces (such as those presented in Fig. 5) to yield significant information is described here. The information of interest is the boundaries between the different regimes of operation and the amplitudes and frequencies of pressure oscillations as functions of L^* and the mean chamber pressure for the different propellants.

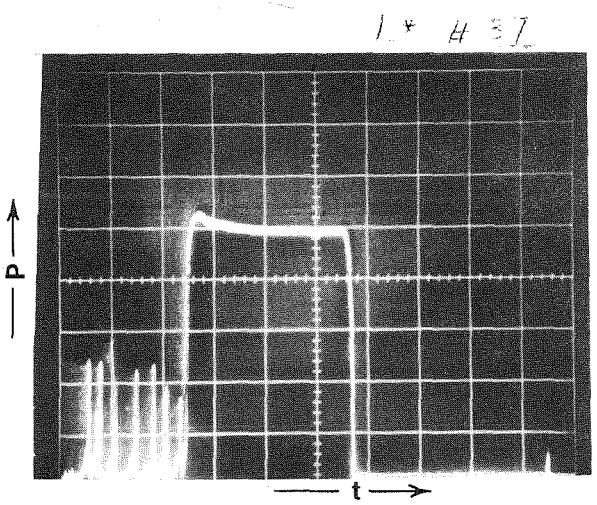

(a) Run No. 37
Propellant: CIT-2
Volume at burnout: 58 cc
L^* at burnout: 89.2 cm
Ignition: a thin layer of ignitor paste over the surface; a small pellet of ignitor paste at the center.

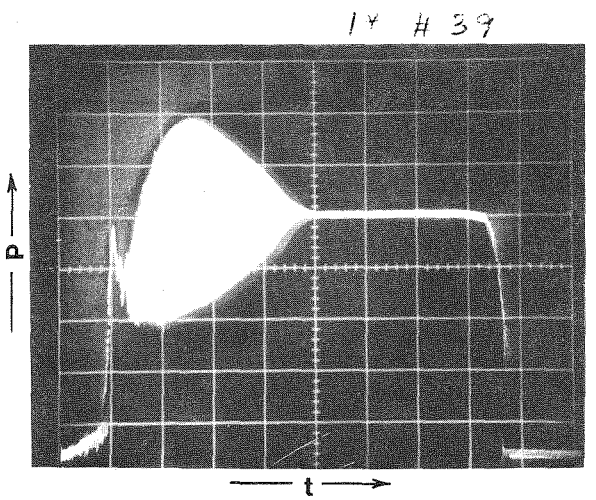

(b) Run No. 39
Propellant: CIT-2
Volume at burnout: 56 cc
L^* at burnout: 86.1 cm
Ignition: a thick layer of ignitor paste over the surface; a large pellet of ignitor paste at the center.

[Oscilloscope sweep speeds were not the same in (a) and (b).]

Figure 10. Influence of Ignition Detail on L-Star Instability.

In Figs. 5a, b, and c the different regimes of the L^* motor operation are highlighted, each in a separate run. However, the goal is always to conduct a test such as the one shown in Fig. 5d, not only because of the wealth of information concentrated in a single run, but also because of the sharply-defined boundaries between the different regimes of combustion. Because of extensive compression along the time axis, the discrete waveforms are not seen in Fig. 5d. Figure 11 shows the time-extended trace in a typical run where the Helmholtz oscillations are extensive. A few cycles after point A, the amplitudes reach their maximum value and these are measured along with the frequency around the maximum amplitude location. Point B represents approximately the midlocation of the Helmholtz mode regime during this run. We remind ourselves that because of propellant consumption as time progresses, the chamber free volume, and hence the characteristic length L^*, increases as time progresses. At point C, the L^* has reached a sufficiently large value for the motor to enter the time-independent regime of operation. That is, point C is the stability boundary for the propellant and represents one point on the $L^* - \bar{P}$ stability map.

In order to know the exact locations of the points of interest (A, B and C) on the L^* scale, it is necessary to have the values of the chamber free volume at these instants. With a knowledge of the speed of data recording, the lengths on the traces are related to the time coordinate. The value of the mean regression rate of the propellant in the chamber is needed to relate this time to the chamber free volume. Ideally, one would use the mean regression rate measured during the run (knowing the initial thickness of the propellant and the run duration). In practice, various difficulties (discussed fully in ref. 6) in the above procedure led to the use of Crawford bomb data (presented in Fig. 2). Care was exercised during the data reduction not to use the Crawford bomb data on the linear regression rates in the calculations pertaining to the chuff mode.

In general, the difficulty in obtaining experimental data increased with the size of the oxidizer particle in the propellant. This difficulty with the coarser oxidizer particle propellants was manifest in two principal characteristics. First, these propellants exhibited a general reluctance to enter the Helmholtz mode instability; second, even if these propellants could be persuaded to enter the Helmholtz mode with careful tailoring of the experimental conditions, the (dp/dt) during the oscillations was often strong enough to extinguish the propellants after only a few cycles. A stability map for the propellant is about the only information that can be obtained from a test unless the propellant enters the Helmholtz mode. (During a firing, the L^* and D^* are known, and the pressure trace reveals whether the firing was stable or unstable. Such information, covering a wide range of L^* and D^*, yields the stability map for the propellant.)

However, unless the pressure trace shows Helmholtz oscillations gradually decaying into the time-independent regime, as shown at C in Fig. 11, the stability boundary cannot be sharply defined. Also, the interesting details of pressure amplitudes, frequencies, and their relation to L^* and the mean chamber pressure cannot be obtained from a pressure trace devoid of Helmholtz oscillations. During the present program, all of the propellants except CIT-4 yielded at least a few runs with extensive Helmholtz oscillations.

The difficulty of exciting the Helmholtz oscillations in the coarser oxidizer particle propellants is believed to hold the key to an understanding of the L^* instability in rockets, as discussed in the subsequent sections.

VI. RESULTS AND DISCUSSION

6.1 Introduction

A thorough understanding of L^* instability in rockets should ultimately result in the elucidation of the variations of any parameter of interest. For the present, we are concerned with those facets that are thought to be fundamental enough to incorporate in them most of the significant information. These are the frequency of oscillations, the stability maps, and the amplitude of pressure oscillations. In the absence of theoretical predictions for these quantities, our success at explaining these phenomena is reflected in reconciliation of experimental data with qualitative physical explanations.

A majority of discussions in this chapter is concerned with the Helmholtz mode oscillations; that is, the segment AC in pressure traces such as Fig. 11. Excluding time-independent combustion (Fig. 5c, for example) of the various pressure-time histories obtained, the Helmholtz mode appears to be the most ordered, and presumably the one most amenable to a theoretical explanation.

The frequency of Helmholtz oscillations is seen to bear a strong relation to the characteristic transit time in the condensed phase, namely, the ratio of the oxidizer particle size to the mean regression rate. Also, simple correlation of the frequency with the chamber characteristic length (L^*) is shown to be limited to each particular propellant only, and to lack universal validity. It is also seen that the oxidizer particle size is a more relevant length scale in the condensed phase than the characteristic thermal depth ($\kappa/\bar{r}$), at least for the Helmholtz oscillations.

The stability maps, which separate regions of time-independent and time-dependent combustion on plots of pressure vs. L-star, are seen to be parabolic in shape, with dual pressure limits for stability in the L^* range of interest. Attempts are made to predict the high pressure limit for unconditional stability. Postulating that the condensed-phase heat reservoir ($c \cdot \Delta T$) effects are important for driving the oscillations, a criterion is sought for classifying the condensed phase as homogeneous or heterogeneous for the purposes of heat transfer calculations. The relative magnitudes of the characteristic thermal depth in the condensed phase and the oxidizer particle size are used for such a criterion. The agreement is found to be excellent for the 11μ (CIT-2) propellant and fair for the 39.5μ ($\tilde{A}$-13) propellant; the agreement is rather poor for the coarser oxidizer (CIT-3 and CIT-4) propellants.

The amplitudes of pressure oscillations are seen to present very difficult problems, even for simple correlations. While several explanations are offered for this difficulty, it is evident that

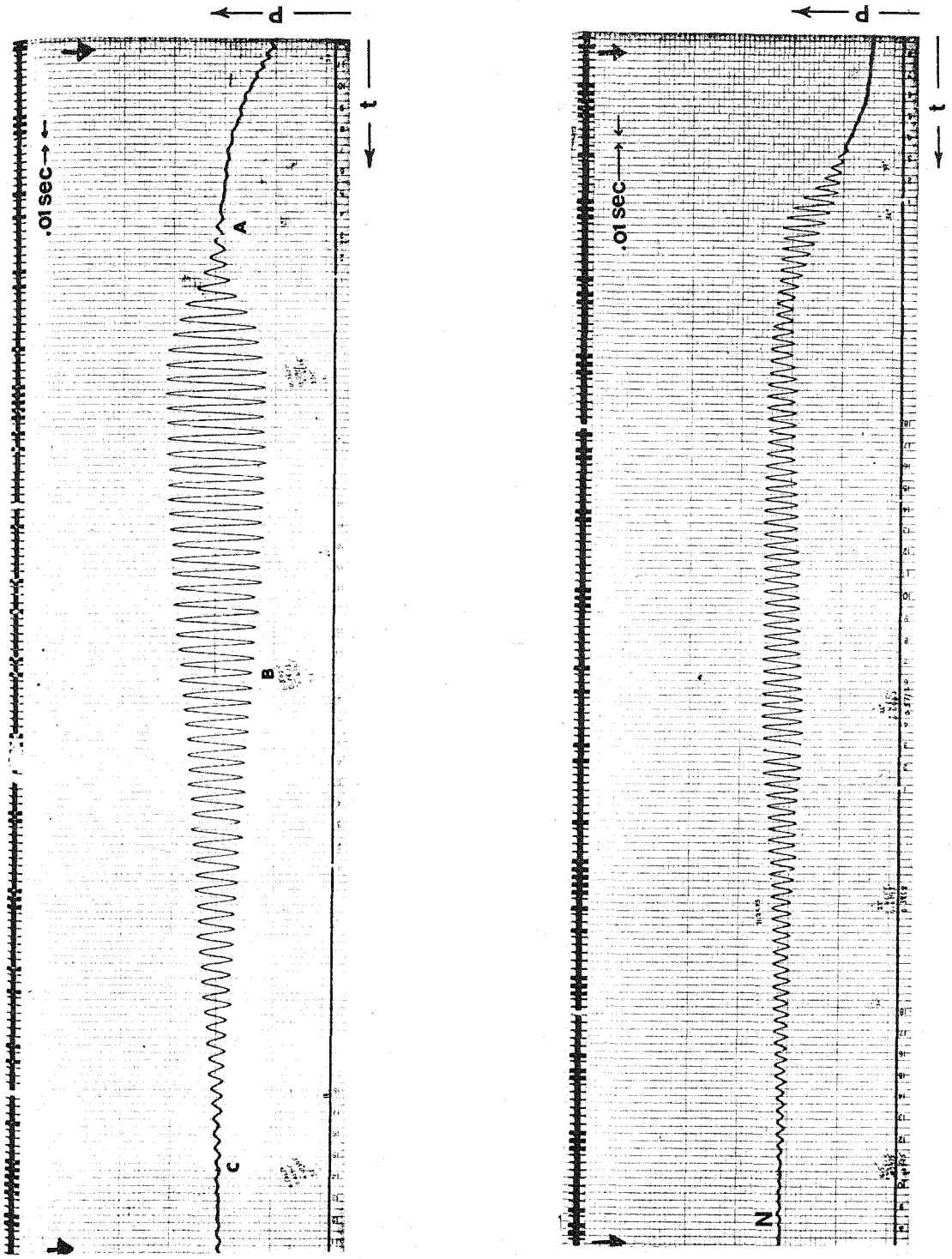

(a) Easily interpreted history (run no. 161, $\bar{P}$ = 32.55 psia, L^* = 60 - 80 cm).

(b) Less certain history (run no. 160, $\bar{P}$ = 28.20 psia, L^* = 50 - 70 cm).

Figure 11. Pressure-Time Traces Obtained on the Oscillograph. Example: $\tilde{A}$-13 Propellant.

more research is needed to clarify matters.

Finally, no attempts are made to compute the response functions from the pressure-time traces. In the L^* burner, the growth of pressure oscillations occurs during progressive decreases in the L^* value, and unless a careful account is taken of this non-stationary nature, the results may not be valid. Since the full growth usually occurs within a few cycles, it is not easy to measure the growth constants, which are meaningful only in the small amplitude (linear) regime. That is, when the growth is spread over a large number of cycles (at least a hundred), the growth constants are readily interpreted. Also, the rapidly varying chamber conditions could introduce large uncer-

tainties in all such interpretations. (The reader will note the similarity to the decay constants measured in T-burners[5], where large uncertainties are present because of the rapidly changing chamber conditions.)

6.2 Frequency of Helmholtz Oscillations

After an extensive study of NAI (Non-Acoustic Instability, or L^* instability in the present terminology) covering 4 different propellants, researchers at the Naval Weapons Center present[7] an unique correlation between the values of the characteristic length, L^*, and frequency of oscillations, f. The correlations (fig. 5.16 in ref. 7) cover data on the different propellants at various chamber pressures. Consequently, one of the first correlations attempted in the present study was a plot of L^* vs. f. Such a plot was prepared (ref. 6) for the four propellants of the present program. It was seen that the correlation is unsatisfactory, although for each particular propellant good correlation was evident. Since our experimental data appear to be at least as good as the NWC data, this lack of correlation indicates in a very simple way that an important effect is being overlooked.

It is apparent that the oxidizer particle size must be the important parameter. This follows from the simple reasoning that the oxidizer particle size is the only parameter that is different among the 4 propellants of the present study. Consequently, the differences in L^* instability behavior must be attributable to it. Proper incorporation of the particle size in the frequency variable is, therefore, expected to improve the correlations.

The normalized frequency ($f\,a/\bar{r}$) incorporates the effects of the particle size naturally. The ordinate L^* is a variable that is far more directly relevant to the vapor phase processes than to the condensed phase processes; L^* should be normalized by another significant length scale in the vapor phase. The only relevant length scale appears to be the flame standoff distance X^*, whose numerical value is not readily accessible. However, the value of X^* scales with the ratio of the thermal diffusivity $\varkappa_{gas}$ (of the combustion gases) to the mean flow velocity $\bar{u}$ above the propellant. Hence, $(L^*\bar{u}/\varkappa_{gas})$ is used as the normalized ordinate. Recognizing that $\bar{u} = \bar{r}(\rho_{solid}/\rho_{gas})$, and that the value of k/c for the gas is not too different from that for the solid, we write

$$\frac{L^*\bar{u}}{\varkappa_{gas}} \propto \frac{L^*\bar{r}}{\varkappa}$$

and use the latter group as the normalized L^*. The values of both $\bar{r}$ and $\varkappa$ are convenient to use in the present context. Nevertheless, the above sequence of relations should always be remembered while examining the correlations to be discussed shortly. In the present report, a constant value of $\varkappa$ is used for all four of the propellants. First, the values of $\varkappa$ are not precisely known for the different propellants, although a value of 0.0011 cm^2/sec is normally taken as reasonably representative of reality. Second, even if the value of $\varkappa$ is found to be different for the propellants, the ordinate $(L^*\bar{r}/\varkappa)$ would not change, as the preceding arguments indicate that $\varkappa$ is introduced only as a convenient substitute for $\varkappa_{gas}$. The value of $\varkappa_{gas}$ should be nearly identical for the four propellants, which are identical in chemical composition. It is noted in passing that other normalizations of L^*, like for example $(L^*f/\bar{u})$, invariably introduce the frequency into the ordinate and their correlations with frequency may not be meaningful.

Before proceeding with the plots, the question of the particle size has to be resolved. It is recalled that the existence of distributions for the particle sizes introduces a degree of arbitrariness (that would be absent with truly unimodal particles). At first, we used the conventional 50 percent wt. average point. An unmistakable improvement parameter ($fa/\varkappa$) proved fruitful. The correlation also indicated that the heterogeneity scale (a) in the propellant is very important for L^* instability. This conclusion naturally points out that the 100 percent wt. average point may be a better choice (for a) than the 50 percent wt. average point. The physically realistic heterogeneity is more readily associated with the a_{100} than with a_{50}, which is, after all, a designation of convenience only. A plot based on $(f\,a_{100}/\bar{r})$ is presented in fig. 12. In comparison with earlier plots, vast improvement is evident, and definitely leads one to believe that a_{100} is the proper length scale of importance in L^* instability.

It now remains to account for the remarkably simple correlation obtained by the NWC researchers. Although they obtained data on four different propellants, three of those propellants used the same oxidizer particle size; the fourth propellant used a bimodal distribution whose weight-average equivalent mean size was not far from those of the other three (table 5.1 in ref. 7). In other words, although various parameters such as the chemical composition, fuel binder, metal content, and the fuel/oxidizer ratio were varied in their study, the single most important parameter (a) was varied little among the four propellants. Thus, the propellants that were "different" in many respects might as well be considered identical so long as we restrict our attention to L^* instability, where the oxidizer particle size appears to be the prime variable.

6.3 The Stability Boundary

The classical characterization of the L^*-instability tendencies of a propellant is simply a map for the propellant where the regions of time-independent combustion are distinguished from the regions of oscillatory (or unsteady) combustion. Normally, the value of L^* is plotted against the mean chamber pressure, P. Such maps are obviously valuable for rocket motor design. In fact, the principal aim at the start of the present program was to obtain the maps for all four propellants in an effort to understand the influences of propellant heterogeneity on combustion stability. Since the mean chamber pressure and the value of L^* at the transition point (C in figs. 11a and 11b) between Helmholtz and time-independent combustion mode are generally known from the experimental data, the maps are prepared easily. Curves representing the loci of such points separate regions of stable and time-dependent combustion of the propellants. As already mentioned, the CIT-4 propellant was the only one (among the four) that did not yield traces such as the ones shown in fig. 11. This fact resulted in obtaining sharp stability boundaries for three of the propellants only. A typical map is presented in fig. 13.

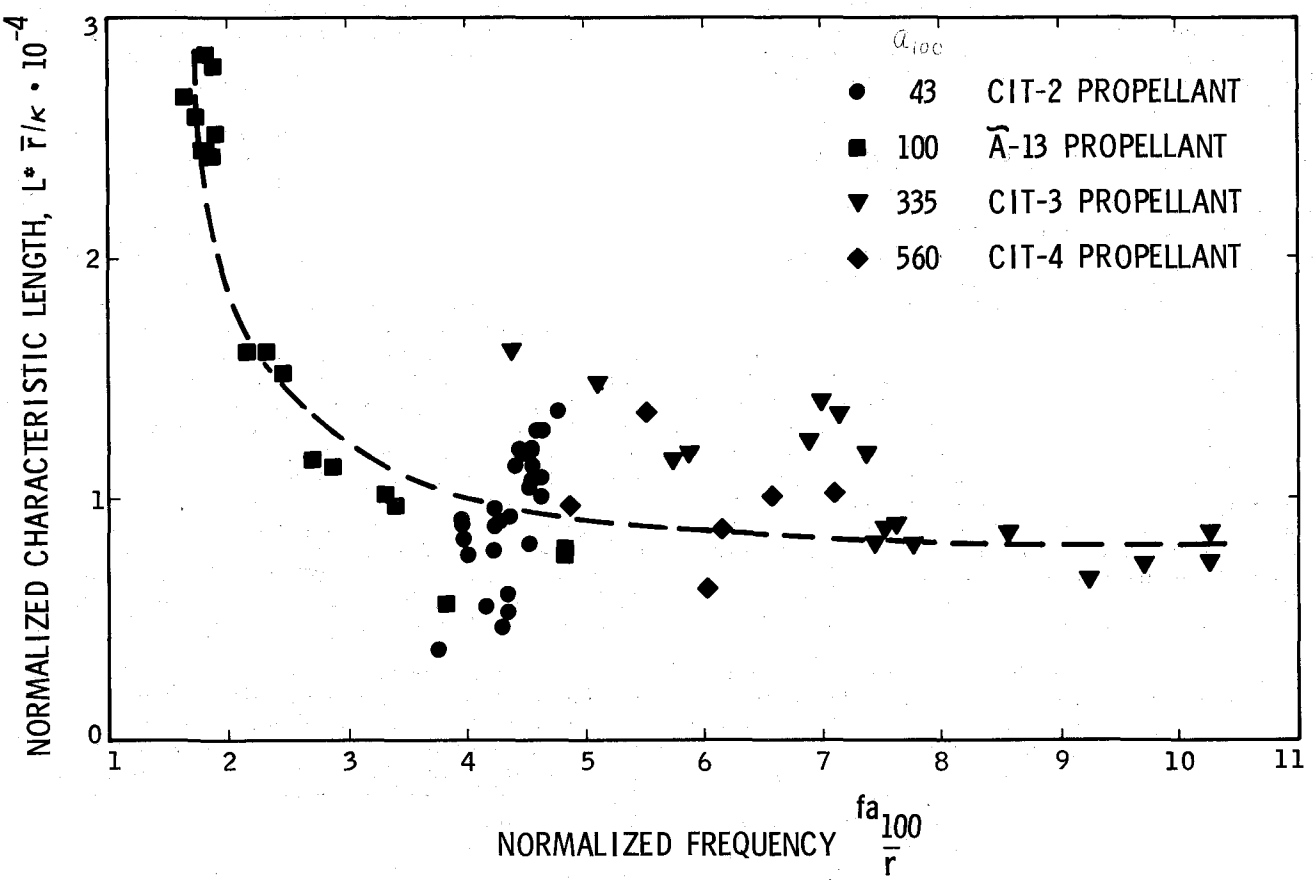

Figure 12. Correlation of the Frequency with L^* for the Propellants

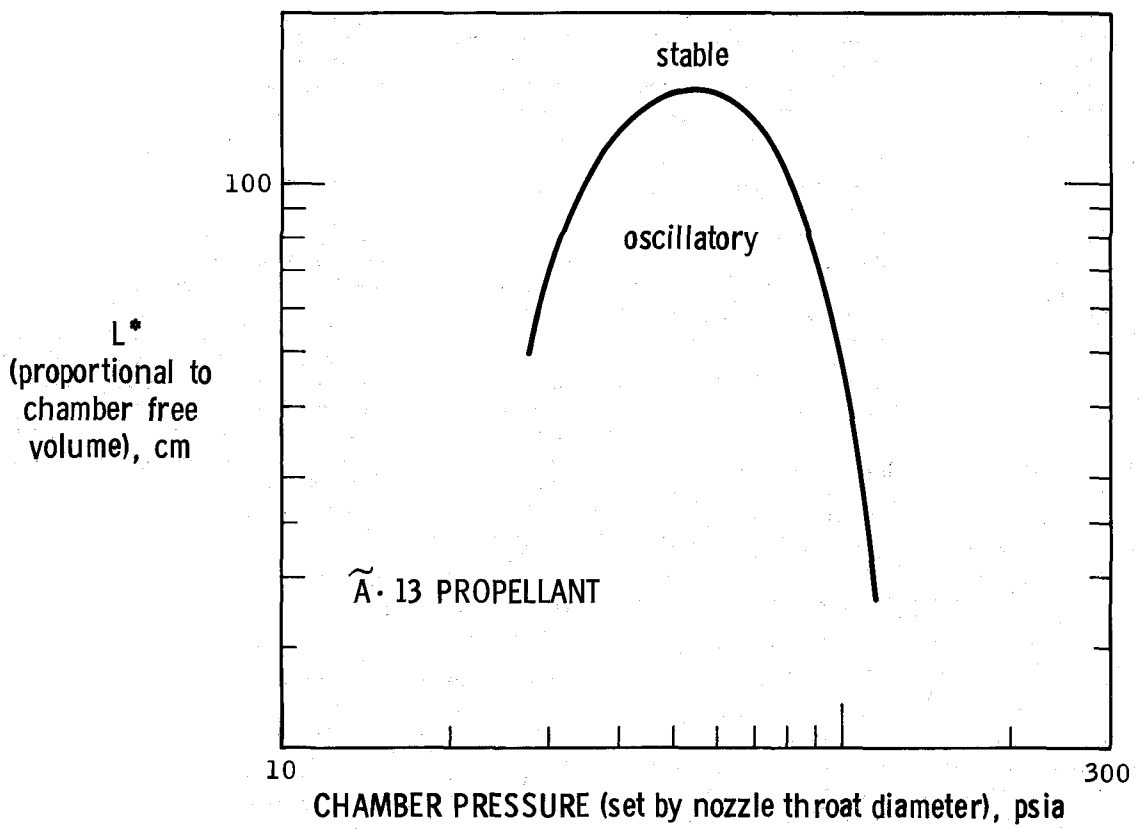

Figure 13. Typical Stability Map

The general characteristic of the stability boundary appears to be a closed region, nearly parabolic in shape, on the $\bar{P}$-L^* plot. Experimental data on the $\tilde{A}$-13 propellant clearly indicate such a boundary (fig. 13). With somewhat lower clarity, the CIT-2 and CIT-3 propellants also indicate such boundaries (ref. 6).

The parabolic shape for the stability boundary is at variance with earlier data[8] that had indicated a straight-line boundary on the log P - log L^* plot. The experiments[8] referred to used a bimodal oxidizer distribution with a different (from PBAN) binder system; however, such details are not expected to alter the qualitative nature of the stability boundary. It would appear that the earlier data[8] covered the high-pressure segment of the parabolic boundary. A straight line is a reasonable approximation for that segment, sufficiently away from the maximum L^* point. The very recent data[9] from ONERA, which clearly indicate the parabolic nature of the stability boundary, provide further support for our experimental results.

While the universal nature of the parabolic boundary has not been conclusively established, at least the high pressure limit has been known for several years. That is, the existence of a mean chamber pressure for each propellant, above which the combustion is time-independent irrespective of the value of L^*. Naturally, an understanding of this phenomenon can be associated with progress towards the delineation of this phenomenon, the approach chosen here is through the condensed phase details. Needless to add, this choice is influenced by the earlier revelation of the important role of the oxidizer particle size during the Helmholtz oscillations (Section 6.2).

Even in the absence of a formal analysis of L^* instability, the role of the condensed phase as a heat reservoir is evident. Temperature fluctuations in the condensed phase, "charge" and "discharge" the reservoir through the c.ΔT effect. This effect, when coupled to the fluctuations in gas phase energetics, can lead to self-sustained oscillations in combustion-related variables. For the condensed phase to act like a good heat reservoir, it would appear that the condensed phase material be homogeneous. By its very nature the composite propellant has come to be regarded as a heterogeneous substance; however, the physical scale of heterogeneity is more relevant than a characterization such as homogeneous/heterogeneous substance. The physical scale of heterogeneity in the propellant is the oxidizer particle size (a).

The physical scale of relevance to heat transfer in the solid is the thermal depth in the propellant material. The mathematical depth appears as infinity, but a distance to reach 1/e of the wall temperature difference ($\bar{T}_w - T_o$) is normally taken as a physically meaningful characteristic depth. Application of the thermal energy equation to the condensed phase, neglecting for simplicity the chemical reactions, yields the solution

$$\frac{\bar{T} - T_o}{\bar{T}_w - T_o} = \exp(-\bar{r}x/\varkappa),$$

so that the distance $x_T = \varkappa/\bar{r}$ is the characteristic depth in the solid.

So long as x_T is greater than the characteristic heterogeneity scale (a), the condensed phase may be considered homogeneous for the purposes of heat transfer calculations. If x_T gets to be comparable to a, it is difficult to visualize the condensed phase as homogeneous for the purposes of heat transfer. Naturally, the heat reservoir effects are expected to be much less pronounced in regimes of operation where

$$(\varkappa/\bar{r}) = x_T \lesssim a .$$

The above arguments show that increasing values of the mean regression rate progressively take the propellant away from the homogeneous-solid limit. (The thermal diffusivity $\varkappa$ is assumed not to vary significantly with the mean regression rate; $\varkappa$ is known to be temperature dependent and the condensed phase temperature near the wall is known not to vary significantly with regression rate.) Since increasing regression rates are generally associated with increasing chamber pressures (i.e., a positive value for the pressure index n like all four of the present propellants have), the preceding reasoning indicates that there should exist a mean pressure for each propellant, above which the instability tendencies are subdued.

In order to verify this reasoning, table I has been prepared. Values of the mean regression rate, above which the instability tendencies are expected to be small, are compared with the values of the mean regression rate ($\hat{r}$) beyond which each propellant is experimentally found to be unconditionally stable in the L^* mode. The value of a_{100} is used instead of a_{50}, since previous developments (Section 6.2) indicate that a_{100} is the physically significant length scale in the condensed phase.

Table I. Comparison of Deduced and Experimental Stability Limit

Propellant	a_{100} cm	$\varkappa/a_{100}$ cm/sec	$\hat{r}$(experimental)
CIT-2	0.0043	0.256	0.266
$\tilde{A}$-13	0.01	0.11	0.295
CIT-3	0.0335	0.0328	0.211
CIT-4	0.0560	0.0197	⟨0.142⟩

As seen in Table I, the agreement for the CIT-2 propellant is very close. There exists an independent observation that strengthens the argument further. When the thermal depth gets to be smaller than the heterogeneity scale in the condensed phase, the steady-state linear regression rate plot is expected to reveal interesting characteristics. For example, surface reactions at the wall are likely to assume greater importance at regression rates greater than $\hat{r}$. If they do, the slope (n) of the Crawford bomb data must undergo a considerable change, as discussed[10] in connection with surface reactions. The Crawford bomb data on the CIT-2 propellant (fig. 2) shows an abrupt break at $\hat{r}$(0.266 cm/sec $\simeq$ 0.105 in/sec). Thus, the CIT-2 propellant seems to fit the thermal-depth picture remarkably well.

The agreement for the $\tilde{A}$-13 propellant (Table II) may be considered reasonable, although the agreement suffers in comparison with the CIT-2 data. Agreement for the CIT-3 and CIT-4 propellants is poor. However, the abrupt break in the Crawford bomb data on the CIT-3 propellant (fig. 2) near a mean regression rate of $\bar{r} = 0.08$ in/sec (≈ 0.204 cm/sec) is remarkably close to the stability limit $\hat{r}$ noted in table II. Naturally, this would seem to indicate the importance of the condensed phase details. Also, it is difficult to believe that the thermal-depth picture can lose its applicability completely, after such a success in explaining the CIT-2 data. A progressive increase in the value of the thermal diffusivity ($\varkappa$) with increases in the material heterogeneity improves the agreement somewhat. But in the absence of accurate data on $\varkappa$ such a hypothesis is purely speculative. However, the slower-burning propellants (coarse oxidizer particle propellants) are likely to have a lower surface temperature, and the $\varkappa$ is known to decrease substantially with temperature, so that the postulated effects of $\varkappa$ variations are not completely ad hoc.

Another explanation is offered for the progressive deterioration in the comparisons noted in table II. As a rule, the low burning-rate propellants are prone to condensed-phase "cooking" before burning. This empirically known effect is supported by theoretical considerations[10] also.

Consider a thin slice (dx in mathematical models) of the propellant that moves from the deep solid (unaffected state, ambient temperature) towards the wall (at high temperature) at the propellant regression rate eigenvalue $\bar{r}$. The lower the regression rate $\bar{r}$, the longer the time that the propellant material spends in the high-temperature regions near the wall; this favors large variations in the physical properties. Until accurate experimental data become available on material properties, covering a wide range of temperature, the above influence is difficult to test, but at least the discussion indicates that uncertainties should increase with coarser oxidizer (lower regression rate) propellants.

Finally, considering the usual uncertainties in such comparisons, the agreement in table II should not be very discouraging.

6.4 The Amplitude of Pressure Oscillations

An understanding of the L^* instability in rockets should result in an acceptable explanation of the amplitude of pressure oscillations. It is to be recognized that we have in question a nonlinear phenomenon, since finite amplitudes are encountered in an isolated system. In the literature on L^* instability, pressure amplitudes are mentioned[11] only rarely. At least a few of the reasons for this negligence will probably become obvious before the end of this section.

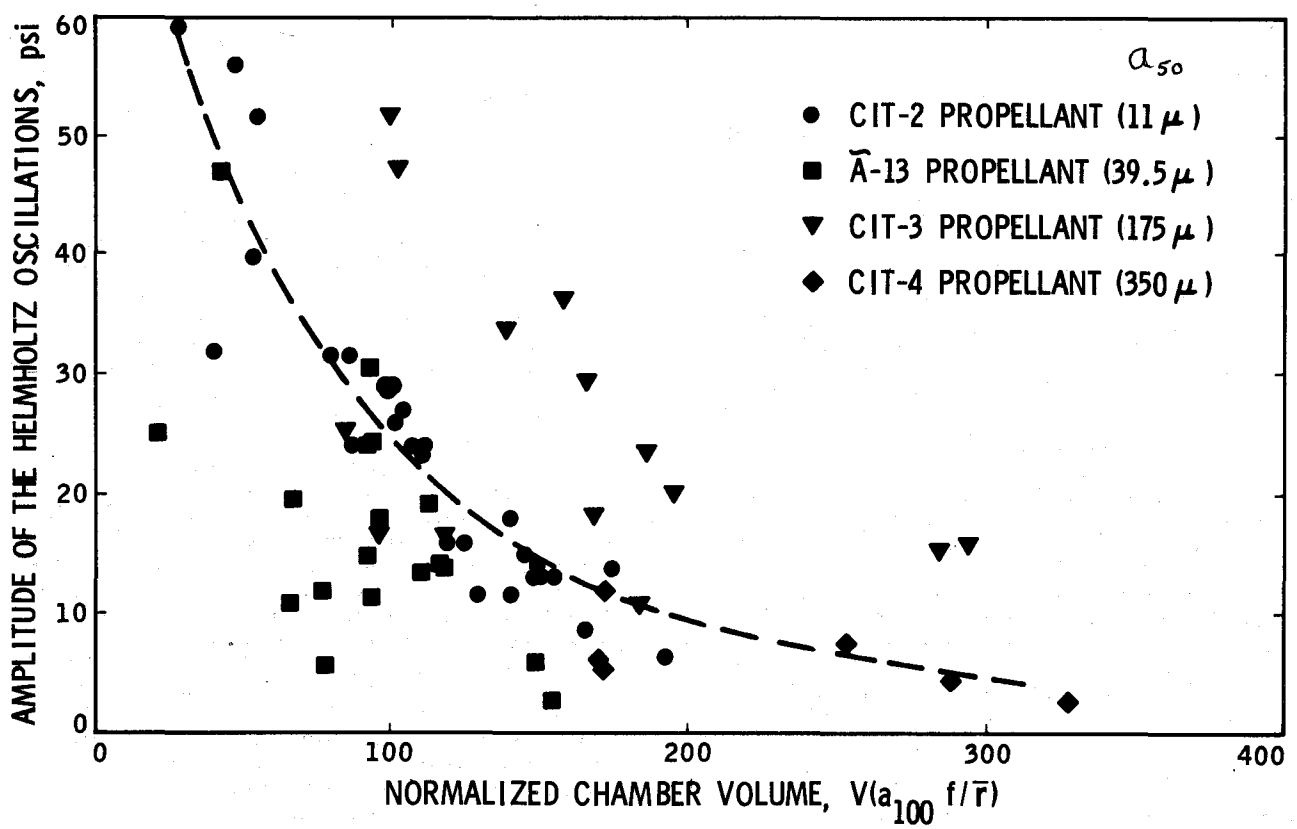

Figure 14. Correlation of the Pressure Amplitude with Volumetric Energy Release Rate

The pressure oscillations are driven by the burning propellant. The fact that the amplitude does not grow indefinitely indicates the simultaneous operation of a loss mechanism. The maximum amplitude observed at any instant is a dynamically controlled parameter in a nonstationary system, and hence the imprecise nature of conventional terminology like "the limiting amplitude" must be clearly recognized. Nevertheless, the amplitude of pressure oscillations is a very important quantity in rocket design. Hence, several correlations were attempted to elucidate possible mechanisms controlling the "limiting amplitude." It is noted that at this stage a completely satisfactory explanation has not been possible. This incomplete success is reflected in correlations that are less than satisfactory.

Various correlations were attempted to bring coherence into the measured pressure amplitudes. All of the attempts, and the reasoning behind those, are discussed in detail in ref. 6. The least unsatisfactory correlation is presented here in fig. 14. The following are three of the possible explanations for the great difficulty encountered in pressure amplitude correlations.

(i) The phenomena are so nonlinear that simple treatments are not meaningful.

(ii) The amplitude, at least during the initial stages in many of the runs, is strongly controlled by the ignition pulse, which is a random variable.

(iii) During many of the runs, the amplitude of pressure oscillations results in cyclic choking and unchoking of the nozzle; this could introduce a new factor of uncertainty.

VII. CONCLUDING REMARKS

This experimental work on L^* instability in solid-propellant rocket motors has yielded a variety of significant information. Many of the observed experimental trends are completely in agreement with anticipations based on qualitative arguments and previous experimental work. However, some of the trends are novel. The following remarks constitute a general summary of the present findings. These remarks are necessarily divided into two classes regarding pertinence to the mode of instability (common to all four of the propellants) and the propellants themselves (compositional variations).

Depending on the combinations of the two primary variables in rocket motor operation (characteristic length, L^*, and the mean pressure, $\bar{P}$), three fundamentally different types of pressure-time histories are observed. These are the chuff mode, Helmholtz mode, and the steady mode. As a slight variation, there exists the pressure burst phenomenon, where the rapidly growing Helmholtz oscillations result in a depressurization-rate (dp/dt) extinguishment of combustion.

Of the three principal modes of L^* instability, the Helmholtz mode is the most ordered. It is one-dimensional in nature. It may be excited only over a narrow range of values of L^* and $\bar{P}$. Besides, even when the $L^* - \bar{P}$ combination permits the Helmholtz mode, a large amplitude pressure disturbance seems to be necessary for its initiation. In general, the frequency of Helmholtz' oscillations decreases with increasing values of L^* for a given propellant. The amplitudes of pressure oscillations during a firing are observed to decrease with increasing L^*; however, this trend is seen to lack generality when a large number of varied firings are considered. Even through the mist of data-scatter associated with the pressure amplitudes, the ratio of chamber free volume to the mean regression rate is seen to be more relevant than the value of L^*.

The chuff mode is far from being one-dimensional. The nozzle is unchoked during most, if not all. of the chuff duration. Severe distortions of the propellant surface and combustion over isolated regions of the surface are evident. The events behind a chuff (pressure spike) are random, and are interpreted only in a statistical sense. Back flow of ambient gases into the chamber is seen as a definite possibility. The initiation of the chuff mode apparently bears a strong relation to the ignition technique. Copious uses of the ignitor paste are seen at times to suppress the chuff mode completely.

The "steady" mode is seen to involve an intrinsic "noise" level of pressure fluctuations. The random amplitude is seen to be nearly independent of the propellant, generally.

The pressure-burst phenomenon is best described as a short-time segment of the more general Helmholtz mode. Preceding the (dp/dt) extinguishment, generally speaking, the mean chamber pressure gradually decreases, although it is not always the case.

The stability boundary for L^* mode is parabolic, with dual values of mean pressure, in the L^* range of interest.

The coarser the oxidizer particles in a propellant, the more difficult it is to obtain data. The coarser oxidizer particle propellants are more difficult to ignite, enter the Helmholtz mode only with great difficulty, and are prone to depressurization-rate extinguishment even under mild conditions. As a corollary, the finer oxidizer particle propellants continue to burn even under severe (dp/dt) transients.

The oxidizer particle size directly controls the frequency of Helmholtz oscillations. On a meaningful relative basis, the coarser the oxidizer particles, the lower the frequency. As far as the particle size itself is concerned, the 100 percent weight average point is more meaningful than the familiar 50 percent weight average point. In the context of Helmholtz oscillations, the oxidizer particle size is a more important parameter than the often-used thermal depth ($\kappa/\bar{r}$) in the solid. In every one of the tests conducted, the value of the parameter (fa_{100}) exceeded the mean regression rate ($\bar{r}$); that is, the important parameter ($f a_{100}/\bar{r}$) was <u>never</u> found to have a value less than unity.

Several of the observed effects (normalized

frequency, high-pressure stability limit, etc.) do not vary monotonically with the oxidizer particle size. For example, the frequency variable $fa_{100}/\bar{r}$) increases in the following order of the oxidizer particle size: 39.5, 11, 350, 175.

When the oxidizer particle size is very fine, the behavior is different from the general trends, even qualitatively. This is amply demonstrated by the data on the CIT-2 (11μ) propellant.

(i) The frequency of Helmholtz oscillations is almost independent of, and increases slightly with, the value of L^* (decreases markedly for the other three propellants).

(ii) The frequency is almost independent of the mean regression rate (generally increases, rather strongly, for the other three propellants).

(iii) The pressure oscillations during the Helmholtz mode are distorted, i.e., possess higher harmonics to a significant degree (almost symmetrical, if not sinusoidal for the other three propellants).

(iv) The noise-level pressure amplitude is practically indiscernible (approximately 1 - 2 psi for the other three propellants).

(v) The amplitudes of the pressure oscillations during the Helmholtz mode correlate very well with the value of L^* (poor correlation with L^* for the other three propellants).

(vi) The high pressure limit for unconditional stability matches excellently with the concept of thermal depth/heterogeneity in the propellant material (fair to poor agreement for the other three propellants).

Throughout the present study, the importance of condensed phase details (exemplified by the oxidizer particle size, characteristic thermal depth in the solid, . . .) is felt in various different forms. These range from the ease of ignition to observed pressure amplitudes, resistance against (dp/dt) extinguishment to correlations of frequency. In general, the more homogeneous the solid, the more readily does the propellant exhibit instability. This general observation is consistent with the feeling that the important role of the condensed phase, in acting like a heat reservoir through the c. ΔT term, is very effective if the solid is homogeneous. Also, attempts to increase the mechanical strength of propellants by adding ingredients that promote a bond between the oxidizer crystals and the binder (thereby increasing the homogeneity of the solid) have resulted in marked increases in the instability behavior. Those experiments will be reported separately; here, it suffices to note the satisfactory trend in agreement with the observations on the present propellants.

To summarize, the oxidizer particle size in the propellant is revealed as an important parameter that has strong influences on L^*-instability behavior.

REFERENCES

1. Green, L. Jr., "Some Effects of Oxidizer Concentration and Particle Size on Resonance Burning of Composite Solid Propellants," Jet Propulsion 28 (March 1958), pp. 159-164.

2. Horton, M. D. and Rice, D. W., "Effect of Compositional Variables upon Oscillatory Combustion of Solid Rocket Propellants," Combustion and Flame, vol. 8, p. 21 (March 1964).

3. Oberg, C. L., "Combustion Instability: the Relationship Between Acoustic and Non-Acoustic Instability," AIAA J. 6, 2, (Feb. 1968), pp. 265-271.

4. Culick, F. E. C., "Some Non-Acoustic Instabilities in Rocket Chambers are Acoustic," AIAA J. 6, 7 (July 1968), pp. 1421-1423.

5. Perry, E. H., "Investigations of the T-burner and its Role in Combustion Instability Studies," Ph. D. Thesis, California Institute of Technology (1970).

6. Kumar, R. N. and McNamara, R. P., "Some Experiments Related to L-Star Instability in Rocket Motors," Daniel & Florence Guggenheim Jet Propulsion Center, California Institute of Technology (March 1973).

7. NOTS TP 4244, "Combustion of Solid Propellants and Low Frequency Combustion Instability," (June 1967).

8. Strand, L., "Low Pressure Combustion Studies," JPL Space Programs Summary 37-41, vol. IV, p. 85 (October 31, 1966).

9. Barrere, M., Nadaud, L., and Lhuillier, J. N., "Survey of ONERA and SNPE work on Combustion Instability in Solid Propellant Rockets," AIAA Preprint No. 72-1052 (1972).

10. Kumar, R. N., "Some Considerations in the Combustion of AP/Composite Propellants," Daniel and Florence Guggenheim Jet Propulsion Center, California Institute of Technology (August 1972).

11. Yount, R. A. and Angelus, T. A., "Chuffing and Nonacoustic Instability Phenomena in Solid Propellant Rockets," AIAA Preprint No. 64-148 (1964).

ACKNOWLEDGMENTS

The authors thank Prof. Fred Culick, Mr. Warren Dowler and Mr. Winston Gin, for their interest in these studies; Mr. Robert Grafius for instrumentation support; Messrs. Leon Strand and Gary Reedy for help during the initial stages; Messrs. Joseph Hance, Larry Ford, Joseph Gurak, Herb Jeffries, Stephen Roche and Fred Tervet for propellant processing and Mr. Anthony Rasmussen for technician help.